

**This is a self-archived version of an original article. This version may differ from the original in pagination and typographic details.**

**Author(s):** Sokolowska, Karolina; Malola, Sami; Lahtinen, Manu; Saarnio, Ville; Permi, Perttu; Koskinen, Katariina; Jalasvuori, Matti; Häkkinen, Hannu; Lehtovaara, Lauri; Lahtinen, Tanja

**Title:** Towards Controlled Synthesis of Water-Soluble Gold Nanoclusters : Synthesis and Analysis

**Year:** 2019

**Version:** Accepted version (Final draft)

**Copyright:** © 2019 American Chemical Society.

**Rights:** In Copyright

**Rights url:** <http://rightsstatements.org/page/InC/1.0/?language=en>

**Please cite the original version:**

Sokolowska, K., Malola, S., Lahtinen, M., Saarnio, V., Permi, P., Koskinen, K., Jalasvuori, M., Häkkinen, H., Lehtovaara, L., & Lahtinen, T. (2019). Towards Controlled Synthesis of Water-Soluble Gold Nanoclusters : Synthesis and Analysis. *The Journal of Physical Chemistry C*, 123(4), 2602-2612. <https://doi.org/10.1021/acs.jpcc.8b11056>

## Towards Controlled Synthesis of Water-Soluble Gold Nanoclusters: Synthesis and Analysis

Karolina Sokolowska, Sami Malola, Manu Lahtinen, Ville Saarnio, Perttu Permi, Katariina Koskinen, Matti Jalasvuori, Hannu Häkkinen, Lauri Lehtovaara, and Tanja Lahtinen

*J. Phys. Chem. C*, **Just Accepted Manuscript** • Publication Date (Web): 07 Jan 2019

Downloaded from <http://pubs.acs.org> on January 8, 2019

### Just Accepted

“Just Accepted” manuscripts have been peer-reviewed and accepted for publication. They are posted online prior to technical editing, formatting for publication and author proofing. The American Chemical Society provides “Just Accepted” as a service to the research community to expedite the dissemination of scientific material as soon as possible after acceptance. “Just Accepted” manuscripts appear in full in PDF format accompanied by an HTML abstract. “Just Accepted” manuscripts have been fully peer reviewed, but should not be considered the official version of record. They are citable by the Digital Object Identifier (DOI®). “Just Accepted” is an optional service offered to authors. Therefore, the “Just Accepted” Web site may not include all articles that will be published in the journal. After a manuscript is technically edited and formatted, it will be removed from the “Just Accepted” Web site and published as an ASAP article. Note that technical editing may introduce minor changes to the manuscript text and/or graphics which could affect content, and all legal disclaimers and ethical guidelines that apply to the journal pertain. ACS cannot be held responsible for errors or consequences arising from the use of information contained in these “Just Accepted” manuscripts.



1  
2  
3  
4  
5  
6 **Towards Controlled Synthesis of Water-Soluble Gold Nanoclusters:**  
7  
8  
9 **Synthesis and Analysis**  
10  
11  
12  
13

14 *Karolina Sokołowska*<sup>1</sup>, *Sami Malola*<sup>2</sup>, *Manu Lahtinen*<sup>1</sup>, *Ville Saarnio*<sup>1</sup>, *Perttu Permi*<sup>1,3</sup>,

15  
16  
17 *Katariina Koskinen*<sup>3</sup>, *Matti Jalasvuori*<sup>3</sup>, *Hannu Häkkinen*<sup>1,2</sup>, *Lauri Lehtovaara*<sup>1</sup> and *Tanja*  
18  
19 *Lahtinen*<sup>1\*</sup>.  
20  
21  
22

23 1 Department of Chemistry, Nanoscience Center, University of Jyväskylä, P.O. Box 35,  
24  
25  
26 40014 Jyväskylä, Finland  
27  
28  
29  
30

31 2 Department of Physics, Nanoscience Center, University of Jyväskylä, P.O. Box 35,  
32  
33  
34 40014 Jyväskylä, Finland  
35  
36  
37  
38

39 3 Department of Biological and Environmental Science, Nanoscience Center, University  
40  
41  
42 of Jyväskylä, P.O. Box 35, 40014 Jyväskylä, Finland  
43  
44  
45  
46  
47  
48  
49  
50  
51  
52  
53  
54  
55  
56  
57  
58  
59  
60

1  
2  
3  
4  
5  
6  
7  
8  
9  
10  
11  
12  
13  
14  
15 **ABSTRACT:** Water-soluble gold nanoclusters with well-defined molecular structure and  
16  
17  
18 stability possess particular biophysical properties making them an excellent candidate  
19  
20  
21 for biological application as well as for fundamental spectroscopic studies. The currently  
22  
23  
24 existing synthetic protocols for atomically monodisperse thiolate-protected gold  
25  
26  
27 nanoclusters (AuMPCs) have been widely expanded with organothiolates yet the direct  
28  
29  
30 synthesis reports for water-soluble AuMPCs are still deficient. Here, we demonstrate a  
31  
32  
33 wet-chemistry pH controlled synthesis of two large water-soluble nanoclusters utilizing  
34  
35  
36 *p*-mercaptobenzoic acid (*p*MBA), affording different sizes of plasmonic AuMPC on  
37  
38  
39 preparative scale (~7 mg). AuMPCs are essentially homogenous in size and are stable  
40  
41  
42 in solution and solid state. Number of characterization methods were used to gain  
43  
44  
45 detailed information about the size, symmetry, molecular composition and structure of  
46  
47  
48 these systems: i.e. HR-TEM, Powder X-ray Diffraction (PXRD), NMR, UV-Vis,  
49  
50  
51  
52  
53  
54  
55  
56  
57  
58  
59  
60

1  
2  
3 Thermogravimetry (TG) and PAGE (Polyacrylamide Gel Electrophoresis). Based on the  
4  
5  
6  
7 conducted experimental analyses and computationally aided predictions it can be  
8  
9  
10 evidenced that both clusters exhibit twinned FCC symmetry with the molecular  
11  
12  
13 composition of  $\text{Au}_{210-230}(\rho\text{MBA})_{70-80}$  and  $\text{Au}_{426-442}(\rho\text{MBA})_{112-115}$ ; referred from now on as  
14  
15  
16  
17 Au250 and Au500, respectively. For future reference, toxicity of both gold clusters in  
18  
19  
20 various concentrations on cultures of gram-positive and gram-negative bacteria was  
21  
22  
23  
24 investigated.  
25  
26  
27  
28  
29  
30  
31  
32  
33  
34  
35  
36  
37  
38  
39  
40  
41  
42  
43  
44  
45  
46  
47

## 48 1. INTRODUCTION

49  
50

51 The unique properties of gold nanoparticles have been studied extensively.<sup>1-4</sup> The  
52  
53  
54 size and shape of the particles define their electronic and physical properties, whereas  
55  
56  
57  
58  
59  
60

1  
2  
3 tuning the nature of the protecting organic layer gives a control of the solubility and  
4  
5  
6  
7 chemical functionality of the particles.<sup>1</sup> The versatile surface chemistry and size-  
8  
9  
10 dependent properties make them universal material in high technology applications  
11  
12  
13 such as sensory probes, electronic conductors, therapeutic agents, drug delivery in  
14  
15  
16  
17 biological and medical applications, and catalysis.<sup>4-11</sup>  
18  
19  
20

21 Colloidal nanoparticles are not well suited for accurate studies of their chemistry. A  
22  
23  
24 typical nanoparticle synthesis produces a polydisperse sample of different sizes,  
25  
26  
27 shapes, and surface structures. Therefore, experiments that require atomic-level control  
28  
29  
30 are extremely difficult to carry out. In this regard, monolayer protected gold clusters  
31  
32  
33  
34 (AuMPCs) are small (usually < 2 nm) nanoparticles with well-defined structures,  
35  
36  
37 consisting of metallic core and protecting ligand layer.<sup>12-14</sup> The structures range from  
38  
39  
40 small more molecular-like species, with quantized electronic transitions, to larger more  
41  
42  
43 nanoparticle-like clusters with hundreds of metal atoms, exhibiting localized surface  
44  
45  
46 plasmon resonance.<sup>3,15,16</sup> Contrary to colloidal gold nanoparticles, AuMPC synthesis  
47  
48  
49 produces a well-organized structure, with a specific number of atoms, similar to a  
50  
51  
52  
53 molecule that has enabled accurate studies of their chemistry, as well as direct  
54  
55  
56  
57  
58  
59  
60

1  
2  
3 comparison of experimental and theoretical results.<sup>17</sup> Currently, many sizes of  
4  
5  
6  
7 organosoluble nanoclusters are widely deployed;<sup>18-23</sup> however the direct syntheses of  
8  
9  
10 larger (> 200 gold atoms) water-soluble nanoclusters are still not yet fully understood.

11  
12  
13  
14 Water-soluble gold nanoclusters were previously reported as universal labeling tools  
15  
16  
17 for the bioimaging due to contrast properties, low toxicity and high solubility. For  
18  
19  
20 example, Au<sub>102</sub>(pMBA)<sub>44</sub> was described as a good tracking candidate for accurate site-  
21  
22  
23 specific covalent conjugation to the viral capsid surface where the covalently bound  
24  
25  
26  
27  
28  
29  
30  
31  
32  
33  
34  
35  
36  
37  
38  
39  
40  
41  
42  
43  
44  
45  
46  
47  
48  
49  
50  
51  
52  
53  
54  
55  
56  
57  
58  
59  
60  
nanoclusters keep the viruses stable, allowing better visualization of their entry in  
complex endosomal structures.<sup>4</sup> The surface properties, particularly the solvent/organic  
interface of pMBA-protected gold clusters, are altered depending on the protonation  
state of the cluster.<sup>1</sup> The clusters become water-soluble only when the carboxylic group  
of pMBA-ligand is deprotonated, which is important aspect for chemical modifications.  
Moreover, water-soluble clusters do not require any toxic solvent treatment, which  
makes them a good candidate for green chemistry approaches, and widen the range of  
applicability to more polar solvents.

1  
2  
3 AuMPCs have a great response to the light at resonant wavelength.<sup>23,24</sup> The  
4  
5  
6  
7 plasmonic and near-infrared absorbance (NIR) is well detectable in deep-tissue  
8  
9  
10 samples. We have previously studied covalently bound multimers of gold nanoclusters  
11  
12  
13 and discovered that the examined system displays coupled plasmonic modes in the NIR  
14  
15  
16 therapeutic spectral window (650-1350 nm) which could be potentially used for imaging  
17  
18  
19 biological samples.<sup>25</sup> Ability to covalently link AuMPC through conductive molecule  
20  
21  
22 opens up new prospects to study fundamental physical properties of molecular  
23  
24  
25  
26  
27 electronic devices and internal motions of the particles and binding ligands.<sup>26</sup> Recently,  
28  
29  
30  
31 Bürgi *et al.* reported successful assembly of Au<sub>25</sub>(SBut)<sub>18</sub> multimers via ligand exchange  
32  
33  
34 and studied electron transfer between clusters.<sup>27</sup> Developments of larger precise  
35  
36  
37  
38 analogs of structures that can be modelled with ab initio (DFT) level of theory could  
39  
40  
41  
42 expand the knowledge of quantum plasmonics and emergence of bulk properties of  
43  
44  
45 metals.  
46  
47  
48

49  
50  
51  
52  
53  
54  
55  
56  
57  
58  
59  
60  
61  
62  
63  
64  
65  
66  
67  
68  
69  
70  
71  
72  
73  
74  
75  
76  
77  
78  
79  
80  
81  
82  
83  
84  
85  
86  
87  
88  
89  
90  
91  
92  
93  
94  
95  
96  
97  
98  
99  
100  
101  
102  
103  
104  
105  
106  
107  
108  
109  
110  
111  
112  
113  
114  
115  
116  
117  
118  
119  
120  
121  
122  
123  
124  
125  
126  
127  
128  
129  
130  
131  
132  
133  
134  
135  
136  
137  
138  
139  
140  
141  
142  
143  
144  
145  
146  
147  
148  
149  
150  
151  
152  
153  
154  
155  
156  
157  
158  
159  
160  
161  
162  
163  
164  
165  
166  
167  
168  
169  
170  
171  
172  
173  
174  
175  
176  
177  
178  
179  
180  
181  
182  
183  
184  
185  
186  
187  
188  
189  
190  
191  
192  
193  
194  
195  
196  
197  
198  
199  
200  
201  
202  
203  
204  
205  
206  
207  
208  
209  
210  
211  
212  
213  
214  
215  
216  
217  
218  
219  
220  
221  
222  
223  
224  
225  
226  
227  
228  
229  
230  
231  
232  
233  
234  
235  
236  
237  
238  
239  
240  
241  
242  
243  
244  
245  
246  
247  
248  
249  
250  
251  
252  
253  
254  
255  
256  
257  
258  
259  
260  
261  
262  
263  
264  
265  
266  
267  
268  
269  
270  
271  
272  
273  
274  
275  
276  
277  
278  
279  
280  
281  
282  
283  
284  
285  
286  
287  
288  
289  
290  
291  
292  
293  
294  
295  
296  
297  
298  
299  
300  
301  
302  
303  
304  
305  
306  
307  
308  
309  
310  
311  
312  
313  
314  
315  
316  
317  
318  
319  
320  
321  
322  
323  
324  
325  
326  
327  
328  
329  
330  
331  
332  
333  
334  
335  
336  
337  
338  
339  
340  
341  
342  
343  
344  
345  
346  
347  
348  
349  
350  
351  
352  
353  
354  
355  
356  
357  
358  
359  
360  
361  
362  
363  
364  
365  
366  
367  
368  
369  
370  
371  
372  
373  
374  
375  
376  
377  
378  
379  
380  
381  
382  
383  
384  
385  
386  
387  
388  
389  
390  
391  
392  
393  
394  
395  
396  
397  
398  
399  
400  
401  
402  
403  
404  
405  
406  
407  
408  
409  
410  
411  
412  
413  
414  
415  
416  
417  
418  
419  
420  
421  
422  
423  
424  
425  
426  
427  
428  
429  
430  
431  
432  
433  
434  
435  
436  
437  
438  
439  
440  
441  
442  
443  
444  
445  
446  
447  
448  
449  
450  
451  
452  
453  
454  
455  
456  
457  
458  
459  
460  
461  
462  
463  
464  
465  
466  
467  
468  
469  
470  
471  
472  
473  
474  
475  
476  
477  
478  
479  
480  
481  
482  
483  
484  
485  
486  
487  
488  
489  
490  
491  
492  
493  
494  
495  
496  
497  
498  
499  
500  
501  
502  
503  
504  
505  
506  
507  
508  
509  
510  
511  
512  
513  
514  
515  
516  
517  
518  
519  
520  
521  
522  
523  
524  
525  
526  
527  
528  
529  
530  
531  
532  
533  
534  
535  
536  
537  
538  
539  
540  
541  
542  
543  
544  
545  
546  
547  
548  
549  
550  
551  
552  
553  
554  
555  
556  
557  
558  
559  
560  
561  
562  
563  
564  
565  
566  
567  
568  
569  
570  
571  
572  
573  
574  
575  
576  
577  
578  
579  
580  
581  
582  
583  
584  
585  
586  
587  
588  
589  
590  
591  
592  
593  
594  
595  
596  
597  
598  
599  
600  
601  
602  
603  
604  
605  
606  
607  
608  
609  
610  
611  
612  
613  
614  
615  
616  
617  
618  
619  
620  
621  
622  
623  
624  
625  
626  
627  
628  
629  
630  
631  
632  
633  
634  
635  
636  
637  
638  
639  
640  
641  
642  
643  
644  
645  
646  
647  
648  
649  
650  
651  
652  
653  
654  
655  
656  
657  
658  
659  
660  
661  
662  
663  
664  
665  
666  
667  
668  
669  
670  
671  
672  
673  
674  
675  
676  
677  
678  
679  
680  
681  
682  
683  
684  
685  
686  
687  
688  
689  
690  
691  
692  
693  
694  
695  
696  
697  
698  
699  
700  
701  
702  
703  
704  
705  
706  
707  
708  
709  
710  
711  
712  
713  
714  
715  
716  
717  
718  
719  
720  
721  
722  
723  
724  
725  
726  
727  
728  
729  
730  
731  
732  
733  
734  
735  
736  
737  
738  
739  
740  
741  
742  
743  
744  
745  
746  
747  
748  
749  
750  
751  
752  
753  
754  
755  
756  
757  
758  
759  
760  
761  
762  
763  
764  
765  
766  
767  
768  
769  
770  
771  
772  
773  
774  
775  
776  
777  
778  
779  
780  
781  
782  
783  
784  
785  
786  
787  
788  
789  
790  
791  
792  
793  
794  
795  
796  
797  
798  
799  
800  
801  
802  
803  
804  
805  
806  
807  
808  
809  
810  
811  
812  
813  
814  
815  
816  
817  
818  
819  
820  
821  
822  
823  
824  
825  
826  
827  
828  
829  
830  
831  
832  
833  
834  
835  
836  
837  
838  
839  
840  
841  
842  
843  
844  
845  
846  
847  
848  
849  
850  
851  
852  
853  
854  
855  
856  
857  
858  
859  
860  
861  
862  
863  
864  
865  
866  
867  
868  
869  
870  
871  
872  
873  
874  
875  
876  
877  
878  
879  
880  
881  
882  
883  
884  
885  
886  
887  
888  
889  
890  
891  
892  
893  
894  
895  
896  
897  
898  
899  
900  
901  
902  
903  
904  
905  
906  
907  
908  
909  
910  
911  
912  
913  
914  
915  
916  
917  
918  
919  
920  
921  
922  
923  
924  
925  
926  
927  
928  
929  
930  
931  
932  
933  
934  
935  
936  
937  
938  
939  
940  
941  
942  
943  
944  
945  
946  
947  
948  
949  
950  
951  
952  
953  
954  
955  
956  
957  
958  
959  
960  
961  
962  
963  
964  
965  
966  
967  
968  
969  
970  
971  
972  
973  
974  
975  
976  
977  
978  
979  
980  
981  
982  
983  
984  
985  
986  
987  
988  
989  
990  
991  
992  
993  
994  
995  
996  
997  
998  
999  
1000

Currently existing synthetic protocols for producing AuMPCs are most extensively carried out using organosoluble ligands; organothiolates, - in particular phenylethanethiol (PET).<sup>18-22,30</sup> The synthesis generally produces a set of



1  
2  
3 heterogeneous particles, requiring etching, size focusing and/or other methods to  
4  
5  
6 narrow size distribution.<sup>18,27-33</sup> The key, to the characteristic stability and the atomically  
7  
8  
9 precise size control of those particles is the role of protecting ligand layer. Covalently  
10  
11  
12 bound ligands govern the kinetic control and thermodynamic selection of the robust  
13  
14  
15 sizes in the synthesis.<sup>3</sup> In contrast to the AuMPCs, the colloidal gold nanoparticles are  
16  
17  
18 typically protected by weakly bound surfactant or even without any protecting ligand  
19  
20  
21 layer, significantly affecting their stability leading to extensive aggregation. For water-  
22  
23  
24 soluble gold nanoclusters, the synthetic control is obtained by precise selection of  
25  
26  
27 reaction conditions, in a way that the single sized product is favored.<sup>34, 35</sup> To produce a  
28  
29  
30 large panel of uniform clusters of chosen sizes, the synthetic parameters of these direct  
31  
32  
33 synthesis methods need to be explored thoroughly.<sup>36</sup> Among several water-soluble  
34  
35  
36 thiols that can stabilize gold nanoclusters, mercaptobenzoic acid (MBA) has been  
37  
38  
39 actively used.<sup>31-41</sup> More specifically, syntheses have been developed for 3-MBA  
40  
41  
42 (*m*MBA)<sup>37-40</sup> and 4-MBA (*p*MBA)<sup>31-36,41,42</sup> protected clusters; e.g. Au<sub>68</sub>(*m*MBA)<sub>32</sub>  
43  
44  
45 Au<sub>144</sub>(*m*MBA)<sub>n</sub> and Au<sub>144</sub>(*p*MBA)<sub>60</sub>, Au<sub>102</sub>(*p*MBA)<sub>44</sub> and Au<sub>146</sub>(*p*MBA)<sub>57</sub>. Among *p*MBA-  
46  
47  
48 stabilized particles, only Au<sub>144</sub>(*p*MBA)<sub>60</sub> and Au<sub>102</sub>(*p*MBA)<sub>44</sub> were synthesized without  
49  
50  
51  
52  
53  
54  
55  
56  
57  
58  
59  
60

1  
2  
3 any size focusing methods, resulting in direct synthesis protocol. In this work, we are  
4  
5  
6  
7 focusing on *p*MBA-stabilized gold nanoclusters to study synthetic parameters of direct  
8  
9  
10 synthesis methods.

11  
12  
13  
14 Precise characterization of individual gold nanoclusters in respect to their composition  
15  
16  
17 and structure has been made by various techniques.<sup>38,40,41</sup> However, despite of  
18  
19  
20 significant development in structure determination techniques within past years, atomic-  
21  
22  
23 level information of clusters bigger than 100 gold atoms is still a grand challenge to  
24  
25  
26  
27  
28 achieve, particularly for water-soluble clusters. Thereby, with lack of information on  
29  
30  
31 structure-properties relationship applicability of the clusters remains limited.

32  
33  
34  
35 In this paper, through the systematic variation of reaction conditions we synthesized  
36  
37  
38 stable, water-soluble *p*MBA-thiolate gold nanoclusters. We found that controlling the pH  
39  
40  
41 in different MeOH/H<sub>2</sub>O conditions produces different sizes of *p*MBA-clusters. To our  
42  
43  
44  
45 knowledge, this is the first straightforward wet-chemistry synthesis to produce larger,  
46  
47  
48 water-soluble *p*MBA-protected gold nanoclusters in milligram scale. Experimental and  
49  
50  
51 theoretical evidence helped us to predict molecular composition of these larger *p*MBA-  
52  
53  
54  
55  
56 clusters to be

1  
2  
3  $Au_{210-230}(\rho MBA)_{70-80}$  and  $Au_{426-442}(\rho MBA)_{112-115}$  referred further on as Au250 (synthesis  
4  
5  
6  
7 previously published by us)<sup>25,42</sup> and Au500, respectively. The synthesized clusters are  
8  
9  
10 stable both in solid and in solution at room temperature for at least six months, as  
11  
12  
13 determined by PAGE and UV-vis analysis. For future studies, the toxicity of both gold  
14  
15  
16 clusters was also studied. As a result, neither Au250 or Au500 caused significant  
17  
18  
19 decrease or elevation in the growth densities of *Bacillus thuringiensis* HER1410,  
20  
21  
22  
23  
24 *Escherichia coli* HB101 or *Klebsiella pneumonia*.  
25  
26  
27  
28  
29  
30  
31

## 32 2. MATERIALS AND EXPERIMENTAL METHODS

### 33 34 35 36 Materials

37  
38  
39  
40 All reagents were commercial and used as received unless otherwise mentioned.  
41  
42  
43  
44

### 45 Synthesis and separation

46  
47  
48  
49  $\rho$ MBA-thiol protected AuMPCs were synthesized under pH controlled conditions.  
50  
51  
52

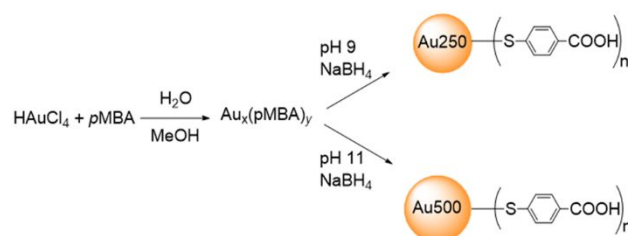
53 Different solvent compositions were used to fine-tune the reduction kinetics of the MPC  
54  
55  
56  
57  
58  
59  
60

1  
2  
3 growth leading to the discrete cluster size (Fig. 1). Smaller nanocluster Au250 was  
4  
5  
6 synthesized at higher pH (around 11) with mixed solvent of 26% MeOH (v/v) in water,<sup>25</sup>  
7  
8  
9  
10 whereas larger nanocluster Au500 was synthesized at slightly lower pH (around 9) and  
11  
12  
13  
14 having solvent mixture of 24% MeOH in water.  
15

16  
17 In a typical synthesis, HAuCl<sub>4</sub> first reacts with excess pMBA-thiol in basic aqueous  
18  
19  
20 solution to form colorless Au(I)SR aggregated complexes. Then, NaBH<sub>4</sub> is added to  
21  
22  
23 reduce Au(I)SR into Au<sub>x</sub>(pMBA)<sub>y</sub>. The synthesis of smaller Au250 nanocluster produces  
24  
25  
26  
27 one single size of AuMPCs. Detailed description of the syntheses and purification are  
28  
29  
30  
31 given in ESI.  
32  
33

34  
35 Due to the lack of crystal structure, several characterization techniques were  
36  
37  
38 conducted to gain detailed information about the size, symmetry, molecular composition  
39  
40  
41 and structure of these systems. The as-obtained products were analyzed using  
42  
43  
44 polyacrylamide gel electrophoresis (PAGE), thermogravimetric analysis (TGA), powder  
45  
46  
47 X-ray diffraction (PXRD), nuclear magnetic resonance spectroscopy (NMR), high  
48  
49  
50 resolution-transmission electron microscopy (HR-TEM), UV-vis spectroscopy, and mass  
51  
52  
53  
54  
55 spectrometry. Unfortunately, all the attempts to measure ESI-MS have not been  
56  
57  
58  
59  
60

successful most likely due to large amount of possible charge states of protective *p*MBA-ligand layer.



**Scheme 1.** Schematic representation of the gold nanocluster synthesis.

**2.1. Polyacrylamide gel electrophoresis (PAGE).** PAGE was run on a 15 % polyacrylamide gel (29:1 acrylamide:bisacrylamide) using 2X TBE run buffer in a Bio-Rad Mini-Protean Tetra System gel electrophoresis apparatus at 130 V.

## Spectroscopy

1  
2  
3  
4 **2.2. Nuclear magnetic resonance (NMR).**  $^1\text{H}$  NMR spectra were recorded on a Bruker  
5  
6  
7 Avance III HD 800 MHz spectrometer, equipped with cryogenically cooled  $^1\text{H}$ ,  $^{13}\text{C}$ ,  $^{15}\text{N}$   
8  
9  
10 triple-resonance PFG Cryoprobe. All spectra were measured at 303 K.

11  
12  
13  
14 **2.3. UV-vis spectroscopy.** The spectra of AuMPCs were measured in  $\text{dH}_2\text{O}$  using  
15  
16  
17 quartz cuvettes and Perkin Elmer Lambda 850 UV/Vis -spectrometer with 2 nm  
18  
19  
20  
21 resolution.

22  
23  
24 **2.4. Thermogravimetric analysis (TG).** Thermal properties of Au-nanoclusters were  
25  
26  
27 examined by Perkin Elmer Pyris 1 thermogravimetric analyzer. TG runs were carried out  
28  
29  
30  
31 in an open platinum pan under air atmosphere (flow rate of 60 ml/min) with a heating  
32  
33  
34 rate of  $10\text{ }^\circ\text{C}/\text{min}$  on temperature range of  $20 - 800\text{ }^\circ\text{C}$ . Analyses were made twice for  
35  
36  
37  
38 each cluster type. Temperature calibration of the analyzer was made by using Curie  
39  
40  
41 transition temperatures of Alumel, nickel, Perkalloy and Fe standards. The weight  
42  
43  
44  
45 balance was calibrated by measuring the standard weight of 50 mg at room  
46  
47  
48  
49 temperature. The sample weights used in the measurements were about 1 – 3 mg.

50  
51  
52 **2.5. Powder X-ray diffraction (PXRD) measurements.** The powder X-ray diffraction  
53  
54  
55  
56 data were measured by PANalytical X'Pert PRO diffractometer in Bragg–Brentano  
57  
58  
59  
60

1  
2  
3 geometry using Cu Ka1 radiation (Johannsson type monochromator;  $\lambda = 1.5406 \text{ \AA}$ ) with  
4  
5  
6  
7 45kV and 40mA power settings. A sample was prepared on a reflection-free silicon-  
8  
9  
10 made plate with an aid of petrolatum jelly. Diffraction patterns were recorded from a  
11  
12  
13 spinning sample by X'Celerator detector using continuous scanning mode in  $2\theta$  range  
14  
15  
16  
17 of  $2 - 140^\circ$  with a step size of  $0.017^\circ$  and with overall data recording time of  $\sim 45$  h per  
18  
19  
20  
21 pattern. Data processing was made with PANalytical HighScore Plus v. 4.7 program  
22  
23  
24 and phase identification data was retrieved from ICDD PD4+ database.<sup>43</sup> Theoretical  
25  
26  
27  
28 powder diffraction curves were calculated as described in Ref. 44.  
29  
30

31 **2.6. High Resolution-Transmission Electron Microscopy (HR-TEM).** HR-TEM samples  
32  
33  
34 were prepared by drop-casting  $8 \mu\text{l}$  of aqueous solution of clusters on a glow discharged  
35  
36  
37  
38 400 mesh lacey carbon copper grid. Solution was allowed to deposit for 15 min, after  
39  
40  
41  
42 which excess sample was removed and washed with water and MeOH. Grid was  
43  
44  
45  
46 allowed to dry overnight. Samples were imaged with 0.2 nm point resolution using JEOL  
47  
48  
49 JEM-2200FS Cs-corrected HR-TEM operated at 200 kV.  
50  
51

52 Simulated HR-TEM images were created from a cluster model with the following  
53  
54  
55  
56 algorithm. A unit vector with random orientation was sampled from uniform angular  
57  
58  
59  
60

1  
2  
3 distribution. Each gold atom in the cluster model was replaced by a Gaussian density  
4  
5  
6  
7 distribution with variance of 1.4 Å, and the density was projected onto the plane defined  
8  
9  
10 by the random unit vector. Finally, the resulting projected density was converted to  
11  
12  
13  
14 grayscale image.  
15  
16

17 **2.7. Prediction of the molecular composition.** Computationally aided predictions of the  
18  
19  
20 molecular composition were done in three ways. In the first approach, theoretically  
21  
22  
23 calculated TG-percentages of the selected structurally known reference systems were  
24  
25  
26  
27 correlated with the number of Au-atoms and the ligands in the systems. In the second  
28  
29  
30 approach, bare Au-cluster models of twinned FCC symmetry were used to estimate the  
31  
32  
33  
34 number of metal atoms in the core of the synthesized clusters. In the third approach,  
35  
36  
37  
38 compositions were predicted by using linear dependence of the number of gold atoms in  
39  
40  
41  
42 the cluster to the volume of the cluster and also by the linear dependence of the number  
43  
44  
45 of ligands to the surface area of the cluster. More detailed information in ESI.  
46  
47  
48

49 **2.8. Bacteria/Toxicity test.** Bacterial biotoxicity of Au<sub>250</sub> and Au<sub>500</sub> were  
50  
51  
52 spectroscopically determined against three bacterial species, *Bacillus thuringiensis*  
53  
54  
55  
56 strain HER1410 (gram-positive), common lab-strain *Escherichia coli* K-12 HB101 (gram-  
57  
58  
59  
60



1  
2  
3 negative) and multidrug-resistant patient isolate *Klebsiella pneumoniae* (gram-negative).  
4  
5  
6

7 All strains were initially cultured in 5 ml of LB medium in + 37 °C and shaken 210 rpm  
8  
9  
10 overnight. Cultures for spectroscopic assay were prepared by adding aqueous solution  
11  
12  
13 of Au250 or Au500 in final concentrations of 0.14 µg/ml, 1.4 µg/ml, 14 µg/ml or 140  
14  
15  
16 µg/ml and 0.13 µg/ml, 1.3 µg/ml, 13 µg/ml or 130 µg/ml, respectively, into 1:1000 diluted  
17  
18  
19 bacterial cultures. Absorbance of bacterial cultures were measured in + 37 °C at 595  
20  
21  
22 nm in 5 minutes intervals for 20 hours in order to determine the bacterial growth and the  
23  
24  
25 maximum population densities. The absorption of Au250, Au500 and growth media was  
26  
27  
28 subtracted from the maximum population densities to measure the bacterial cell  
29  
30  
31 induced absorption under different Au250 and Au500 exposures. Each measurement  
32  
33  
34  
35 was conducted three times.  
36  
37  
38  
39  
40  
41  
42  
43  
44

### 45 3. RESULTS AND DISCUSSION

46  
47  
48 3.1 Synthesis products. Two parameters, pH and MeOH concentration affected the  
49  
50  
51 outcome of the synthesis. Au nanoclusters were synthesized by pH control in different  
52  
53  
54 MeOH composition yielding two different discrete products of stable water-soluble  
55  
56  
57  
58  
59  
60

1  
2  
3 cluster protected by *p*MBA-thiol in milligram scale. These syntheses does not involve  
4  
5  
6  
7 any additional size-focusing step and in case of Au250 the synthesis produces only one  
8  
9  
10 discrete size of particle. Additionally, Au<sub>102</sub>(*p*MBA)<sub>44</sub> nanocluster was synthesized as a  
11  
12  
13  
14 good reference point to compare synthetic trends, dispersity and size of the particles.  
15  
16  
17 The reference Au<sub>102</sub>(*p*MBA)<sub>44</sub> nanocluster was synthesized following previously reported  
18  
19  
20 synthesis.<sup>34</sup> The polymerization step requires relatively high pH of ~13 and conditions of  
21  
22  
23  
24 47% of MeOH. To enable facile comparison of the reaction conditions, we divided the  
25  
26  
27 reaction protocols into 3 stages to extract the information on direct synthesis conditions.  
28  
29  
30  
31 The first stage involves polymerization process, second stage reduction and the last  
32  
33  
34 one purification (Table 1).  
35  
36  
37

38 To synthesize smaller Au250 nanoclusters, HAuCl<sub>4</sub> and *p*MBA-thiol were dissolved in  
39  
40  
41 methanol and mixed, leading to the formation of white precipitate. The initial  
42  
43  
44 Au<sub>x</sub>(*p*MBA)<sub>y</sub> polymerization step requires treatment at a pH of ~11 prior to reduction  
45  
46  
47 nucleating the growth of the metal core. After reduction of Au(I)-*p*MBA precursors with  
48  
49  
50 NaBH<sub>4</sub>, excess of methanol is added and the reaction is quenched producing one  
51  
52  
53  
54  
55 discrete size of particle.  
56  
57  
58  
59  
60

1  
2  
3 Lowering the pH, larger Au500 nanocluster was found. H<sub>2</sub>AuCl<sub>4</sub> and *p*MBA-thiol were  
4  
5  
6 dissolved in 86 % of methanol forming rapidly white precipitate, which was dissolved at  
7  
8  
9  
10 pH ~9. The final product still contains polydisperse clusters mixture, similar to the  
11  
12  
13 Au<sub>102</sub>(*p*MBA)<sub>44</sub> synthesis, and requires fractional precipitation. The separation is done  
14  
15  
16 at 25 % of methanol and centrifuged at 5000 g for 15 mins. Next, the supernatant is  
17  
18  
19  
20 adjusted to 80 % methanol and centrifuged. The pellet from precipitation at 80 %  
21  
22  
23  
24 methanol is the final product.  
25  
26

27 The pH value of the *p*MBA-cluster effects its protonation state and surface properties. The  
28  
29 solvent/organic interface of protecting ligand can be easily altered becoming water-soluble when  
30  
31 the carboxylic group of *p*MBA-ligand is deprotonated and methanol-soluble when protonated.  
32  
33 At the same time, by tuning the pH value during polymerization step the size of the cluster can  
34  
35 be controlled. Larger, Au500 cluster favors slightly lower but still alkaline pH 9, and low MeOH  
36  
37 concentration of 25%. Whereas, Au250 was synthesized at pH 11 and the solvent mixture of  
38  
39 28% (v/v) MeOH in water.  
40  
41  
42  
43

44 When dissolved in water the new products display different colors (yellowish,  
45  
46 brownish, reddish) indicating that they have different sizes. The syntheses of both sizes  
47  
48  
49 produced mg-quantities (~7 mg) of solid material. Each reaction product was analyzed  
50  
51  
52  
53  
54  
55  
56  
57  
58  
59  
60

using polyacrylamide gel electrophoresis (PAGE) and based on the initial size estimation they were assigned as Au250 and Au500, respectively.

Recently, Azubel and Kornberg reported that apart from the thiol-to-gold ratio the size and uniformity of *m*MBA gold particles is highly dependent on adjustment of pH.<sup>37</sup> In contrast to 4-MBA (*p*MBA), *m*MBA ligand induces different properties for the Au-nanocluster mainly due to the meta-position of the acidic group in the phenyl ring, thus resulting in dissimilar ligand orientation and geometry.<sup>39</sup> Nevertheless, smaller *m*MBA clusters of 68 and 144 gold atoms were synthesized at pH 13.<sup>37</sup> In case of 4-MBA clusters the Au<sub>102</sub>(*p*MBA)<sub>44</sub> (Au102) is synthesized also at pH 13 and these larger ones Au250 and Au500 by lowering the pH from 11 to 9. The synthesis conditions for smaller water-soluble MBA-protected nanocluster seem to favor high pH condition.

**Table 1.** Synthesis protocols of *p*MBA-protected gold nanoclusters. The values in columns 2<sup>nd</sup>, 3<sup>rd</sup>, 7<sup>th</sup> correspond to the molar ratios.

	polymerization				reduction		purification
Nanoclusters	<i>p</i> MBA	HAuCl <sub>4</sub>	MeOH %	pH	MeOH %	NaBH <sub>4</sub>	MeOH %

Au102	3	1	47	13	47	1.1	60
Au250	6	1	28	11	26	1.8	pure product without fractional precipitation
Au500	6	1	25	9	25	1.8	25

**3.2. Characterization of AuMPCs.** The size range information of the crude product was preliminarily acquired from their mobility in PAGE gel (Figure 2). The size information and number of gold atoms per product were further examined with HR-TEM. Determined Au contents were further used for estimating number of ligands by thermogravimetry. With UV-vis spectroscopy new insight into size-dependent evolution of surface plasmon resonance (Figure 3) was obtained. Powder X-ray diffraction (PXRD) technique was used to validate the structural features that were obtained by HR-TEM. Finally, based on all the gathered data about the size, symmetry, molecular composition and structure of these clusters, computational prediction was developed for representing structural features of water-soluble  $\mu$ MBA-protected Au250 and Au500 nanoclusters.

1  
2  
3  
4 **PAGE** Dispersity and the size of the prepared AuMPCs were compared to the  
5  
6  
7 reference cluster  $Au_{102}(pMBA)_{44}$  (Figure 1 and S1). The products formed by wet-  
8  
9  
10 chemistry approach showed up as a single well-defined band in PAGE indicating  
11  
12  
13 monodispersity of AuMPCs. The particles were initially analyzed by determination of  
14  
15  
16 electrophoretic mobility. Both products had lower mobility than  $Au_{102}(pMBA)_{44}$  in the  
17  
18  
19 same PAGE run indicating larger sized clusters. Using Au102 as a reference sample,  
20  
21  
22 retention factors ( $r_f$ ) were determined to be 0.77 and 0.64 for Au250 and Au500,  
23  
24  
25 respectively. The products possess stability both in solid and in solution at room  
26  
27  
28 temperature for at least six months, as determined by PAGE and UV-vis analysis.  
29  
30  
31  
32  
33  
34  
35  
36  
37  
38  
39  
40  
41  
42  
43  
44  
45  
46  
47  
48  
49  
50  
51  
52  
53  
54  
55  
56  
57  
58  
59  
60



1  
2  
3  
4 **Figure 1.** PAGE bands of the Au102, Au250 and Au500 nanoclusters.  
5  
6  
7  
8  
9

10 **HR-TEM** images of the AuMPCs were acquired by Gatan software, which was also  
11  
12 used to determine diameter of selected particles (Figure 2 and S2, S3, S4). The biggest  
13  
14 challenge in HR-TEM measurements is its interpretation due to the number of  
15  
16 interferences (and low signal-noise ratio when measuring at atomic resolution). Therefore,  
17  
18 edge-to-edge particle size determination is often difficult. The diameters in the figure 2  
19  
20 correspond to the maximum limit of the size, in other words, the size with error limit 0.1  
21  
22 nm. We estimated the diameter of the smaller product to be  $1.7\pm 0.1$  nm, which fits to  
23  
24 our previously reported size estimation<sup>25</sup> that was based on Gaussian fit from low-  
25  
26 resolution TEM images, yielding the diameter in range of  $1.6\pm 0.3$  nm (Figure 2a). The  
27  
28 metal core diameter of the larger product was determined to be  $2.2\pm 0.1$  nm (Figure 2b,  
29  
30  
31  
32  
33  
34  
35  
36  
37  
38  
39  
40  
41  
42  
43  
44  
45 S4).  
46  
47  
48  
49  
50  
51  
52  
53  
54  
55  
56  
57  
58  
59  
60

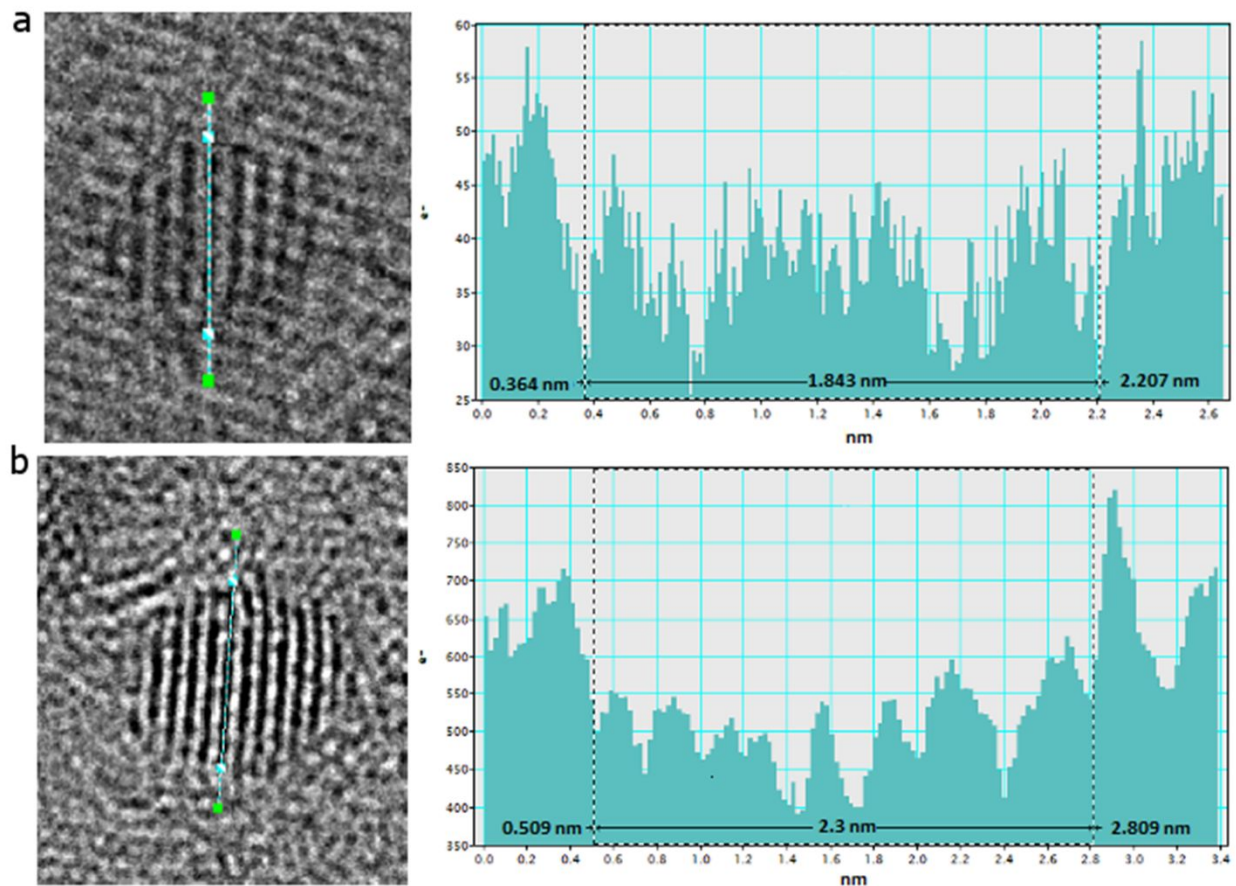
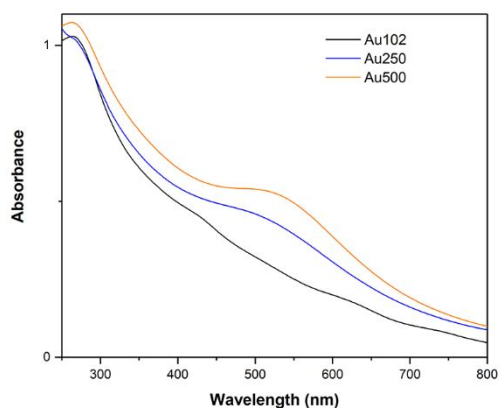


**Figure 2.** HR-TEM images of the assumed a) Au<sub>250</sub> and b) Au<sub>500</sub> *p*MBA-protected nanoclusters. Right panel corresponds to the histogram showing the upper size of the selected particle on the left panel.

**UV-vis** The optical spectra obtained from the two clusters were also compared to the reference spectrum of Au<sub>102</sub>(*p*MBA)<sub>44</sub> (Fig. 3). In contrast to the Au<sub>102</sub>(*p*MBA)<sub>44</sub>, both clusters exhibited an absorption peak at 530 nm which is consistent to the surface plasmon resonance (SPR).<sup>23</sup> With an increase in cluster size, the SPR features



1  
2  
3 increase. The same properties were observed in case of Au250 and Au500 clusters. As  
4  
5  
6  
7 far as we know, prepared particles are the biggest water-soluble nanoclusters  
8  
9  
10 synthesized by direct chemical approaches and demonstrating SPR. The spectrum of  
11  
12  
13 Au250 is compatible to the recently published spectra of 51 kDa,<sup>33</sup> 45 kDa<sup>23</sup> and 53 kDa  
14  
15  
16 clusters,<sup>23</sup> with the estimated number of gold atoms at 250, 226, and 253, respectively.  
17  
18  
19  
20  
21 In case of Au500, the absorption spectrum is compatible with reported spectra of 75  
22  
23  
24 kDa<sup>23</sup> and 88 kDa clusters<sup>33</sup> with estimated gold atoms at 356 and 459.  
25  
26  
27  
28  
29  
30  
31  
32



33  
34  
35  
36  
37  
38  
39  
40  
41  
42  
43  
44  
45  
46  
47 **Figure 3.** UV-vis spectra of Au102 (black), Au250 (blue) and Au500 (orange) clusters in  
48  
49  
50 dH<sub>2</sub>O. A distinct absorption feature corresponding to a LSPR is observed at 530 nm for  
51  
52  
53  
54 the Au250 and Au500 nanoclusters.  
55  
56  
57  
58  
59  
60

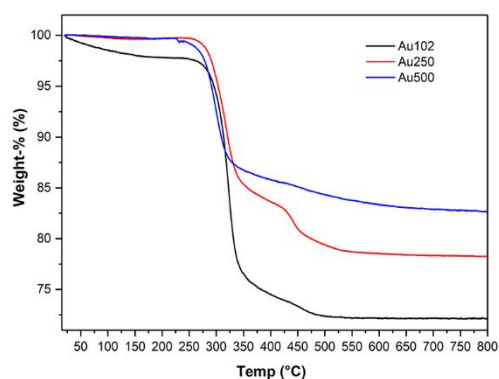
1  
2  
3  
4  
5  
6 **<sup>1</sup>H NMR.** <sup>1</sup>H spectrum of Au250 and Au500 exhibit a typical broad signal for gold  
7  
8  
9 clusters between 5.2 - 9.2 ppm (Figure S5). Additionally two sharp signals (doublets)  
10  
11  
12 can be seen at 7.60 and 7.79 ppm in both spectra, which fit to free *p*MBA-ligand.  
13  
14  
15 However, the <sup>1</sup>H spectrum of Au500 shows additional fine structure in comparison to  
16  
17 Au250, which is relatively featureless. Without considering the free *p*MBA signals, the  
18  
19 Au500 spectrum shows 14 doublet signals (7.92, 7.82, 7.70, 7.65, 7.34, 7.30, 7.14,  
20  
21  
22 6.66, 6.62, 6.55, 6.51, 6.25, 6.19 and 5.79 ppm) and a singlet at 7.61 ppm. These peaks  
23  
24  
25  
26  
27  
28  
29  
30 are characteristic for Au500 nanocluster, but it is still not clear whether they belong to  
31  
32  
33 the cluster structures. In different synthesis products, they appear at the same positions,  
34  
35  
36  
37  
38  
39  
40  
41  
42  
43  
44  
45  
46  
47  
48  
49  
50  
51  
52  
53  
54  
55  
56  
57  
58  
59  
60 but with varying intensities.

**Thermogravimetric analysis (TG).** The weight loss of organic substance upon heating  
is commonly used to estimate the number of ligands in monolayer protected gold  
clusters (the image of the Au residuals after a TG run, see S6). Thermal stability and  
number of organosulfur ligands on the Au<sub>*n*</sub> nanoclusters (*n* = 102, 250, 500) were

1  
2  
3 examined by thermogravimetric analyses (TG). In figure 4, recorded TG curves show  
4  
5  
6  
7 gently descending weight loss (sample dependently 0.4 – 2 wt.-%) from 20 up to about  
8  
9  
10 200 °C (Table 2) that is caused by gradual evaporation of residual surface bound  
11  
12  
13 water. Thermal decomposition of all three Au-clusters initiate slowly above 220 °C  
14  
15  
16 followed by major weight loss from 270 °C to 500, 600 and 700 °C along with an  
17  
18  
19 increase in the size of the Au-cluster. The observed weight losses of the major steps  
20  
21  
22 correspond to thermal decomposition processes and/or desorption of surface ligands  
23  
24  
25 (pMBA), and were determined to be 25.92, 21.32 and 19.60 wt.-% for Au102, Au250  
26  
27  
28 and Au500 clusters, respectively (Table 2).  
29  
30  
31  
32  
33  
34

35 The number of surface ligands can be estimated via the observed residual weight of  
36  
37  
38 each TG run (74.08, 78.68, and 83.11% for Au102, Au250 and Au500, respectively) by  
39  
40  
41 calculating those as moles of Au. The number of gold atoms used here are based on  
42  
43  
44 computationally aided predictions explained in detail later in the section 3.4. The original  
45  
46  
47 molar mass of the  $Au_x(SR)_y$  cluster can then be calculated based on the expected 1 to 1  
48  
49  
50 stoichiometry between the gold containing residual and the original  $Au_x(SR)_y$  cluster,  
51  
52  
53  
54  
55  
56 from which the number of surface ligands  $(SR)_y$  can then be evaluated by taking into  
57  
58  
59  
60

1  
2  
3 account the molar mass of the (SR) ligand. Functionality of the method was confirmed  
4  
5  
6  
7 by the reference cluster Au102 for which  $45 \pm 1$  surface ligands is determined by the  
8  
9  
10 analysis, agreeing well to number of the ligands (44) reported in the single crystal  
11  
12  
13 structure of the cluster by Jadzinsky *et al.*<sup>45</sup> Similarly, 73-80 and 111-116 surface  
14  
15  
16 ligands were determined for Au250 and Au500 clusters, respectively. Determined  
17  
18  
19 number of ligands match also remarkably well to those obtained by our computational  
20  
21  
22  
23  
24  
25  
26  
27  
28  
29 predictions (see section 3.4).



30  
31  
32  
33  
34  
35  
36  
37  
38  
39  
40  
41  
42 **Figure 4.** TG curves of Au102, Au250 and Au500 clusters measured with a heating rate  
43  
44  
45  
46 of 10 °C/min under air atmosphere.

**Table 2.** TG results for Au102, Au250 and Au500 nanoclusters.

Sample name	1 <sup>st</sup> weight loss <sup>a</sup> (%)	Temp. (°C)	2 <sup>nd</sup> weight loss <sup>b</sup> (%)	Temp. (°C)	Residual <sup>c</sup> (%)	No. of ligands	No. of Au atoms
Au102	2.13	24 - 214	25.92	214 - 800	74.08	45	102
Au250	0.37	24 - 190	21.32	190 - 800	78.68	73 - 80	210 - 230
Au500	0.40	24 - 192	16.90	192 - 800	83.11	111 - 116	426 - 442

a = residual water, b = ligand removal, c = residual weight corresponding to gold content

**Toxicity on bacteria** Neither Au250 nor Au500 caused significant decrease or elevation in the growth densities of *Bacillus thuringiensis* HER1410, *Escherichia coli* HB101 or *Klebsiella pneumoniae* in concentrations 0.14 – 14 µg/ml of Au250 or 0.13 – 13 µg/ml of Au500 (Figure 5). In higher concentrations (140 µg/ml and 130 µg/ml) the self-absorption of Au250 and Au500 obscured the optical density of the cultures and thus the changes in bacterial growth could not be reliably observed. Nevertheless, based on the results, Au250 and Au500 do not seem to affect bacterial viability.

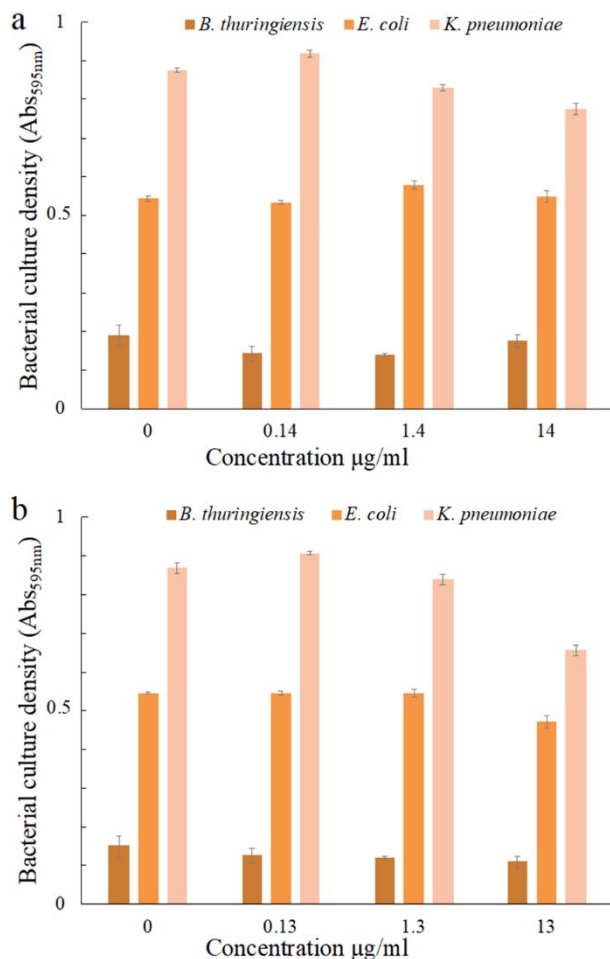


**Figure 5.** Spectroscopic biotoxicity assay of gold nanoclusters a) Au250 and b) Au500 on bacterial species *Bacillus thuringiensis*, *Escherichia coli* and *Klebsiella pneumoniae*.

Maximum absorption (595 nm) of bacterial cultures were measured in the presence of either Au250 or Au500 in different concentrations during 20 h cultivation (N=3). The slight decline of absorbance in the highest concentration was due to increasing background absorption. Error bars: standard deviation.

### 3.3. Exploring the atomic structure

Before predicting the molecular compositions of the clusters, we first present a short discussion on the structural patterns of water-soluble *p*MBA-protected cluster systems. We compare measured powder X-ray diffraction results of the synthesized clusters to the symmetries of selected, structurally known, thiolate protected clusters. We also present a range for possible basis for metal core structure of Au<sub>250</sub> and Au<sub>500</sub> nanoclusters based on experimental and theoretical data.

#### Powder X-ray diffraction (PXRD) analysis

Comparison of the experimental XRD patterns of Au<sub>250</sub> and Au<sub>500</sub> nanoclusters to the calculated reference systems of Au<sub>146</sub>(*p*MBA)<sub>57</sub>, Au<sub>246</sub>(SC<sub>6</sub>H<sub>4</sub>CH<sub>3</sub>)<sub>80</sub> and Au<sub>279</sub>(TBBT)<sub>84</sub> is illustrated in Figure 6. The Au<sub>246</sub> nanocluster displays the decahedral core and Au<sub>146</sub>(*p*MBA)<sub>57</sub> represents the largest so far solved water-soluble cluster with FCC-based twinned core.<sup>41</sup> The XRD patterns of both clusters show the strongest diffraction peak at ~40° 2θ, two relatively broad peaks at ~60 - 80° 2θ and some minor peaks at ~45° and ~50° 2θ. With phase identification routine, the observed diffraction

1  
2  
3 peaks are characteristic for gold phase crystallizing in cubic face-centered crystal  
4  
5  
6  
7 system and no additional unindexed peaks remain in the patterns (large hump 15 - 20°  
8  
9  
10 and very sharp peak at 21.4° 2θ originates from a sample holder/adhesive substance)<sup>43</sup>.

11  
12  
13 The calculated XRD pattern of Au<sub>146</sub>(pMBA)<sub>57</sub> is remarkably similar to the experimental  
14  
15  
16 data of Au250 and Au500 clusters. As the diffraction peaks at 38.8°, 66.2° and 75.7° in  
17  
18  
19 both experimental patterns have similar shape features and are located at the equal  
20  
21  
22 diffraction angles than that of in Au146 pattern. Instead, the simulated patterns of  
23  
24  
25  
26  
27  
28  
29  
30  
31  
32  
33  
34  
35  
36  
37  
38  
39  
40  
41  
42  
43  
44  
45  
46  
47  
48  
49  
50  
51  
52  
53  
54  
55  
56  
57  
58  
59  
60  
Moreover, the peak maximums of the main peaks in Au246 and Au279 are also  
somewhat shifted to lower 2θ angles and the shape properties of the peaks are subtly  
different. Described observations suggest that the metal core of both Au250 and Au500  
nanoclusters most likely adopts the FCC symmetry, which is also twinned as indicated  
by the computational analyses represented in following chapters.



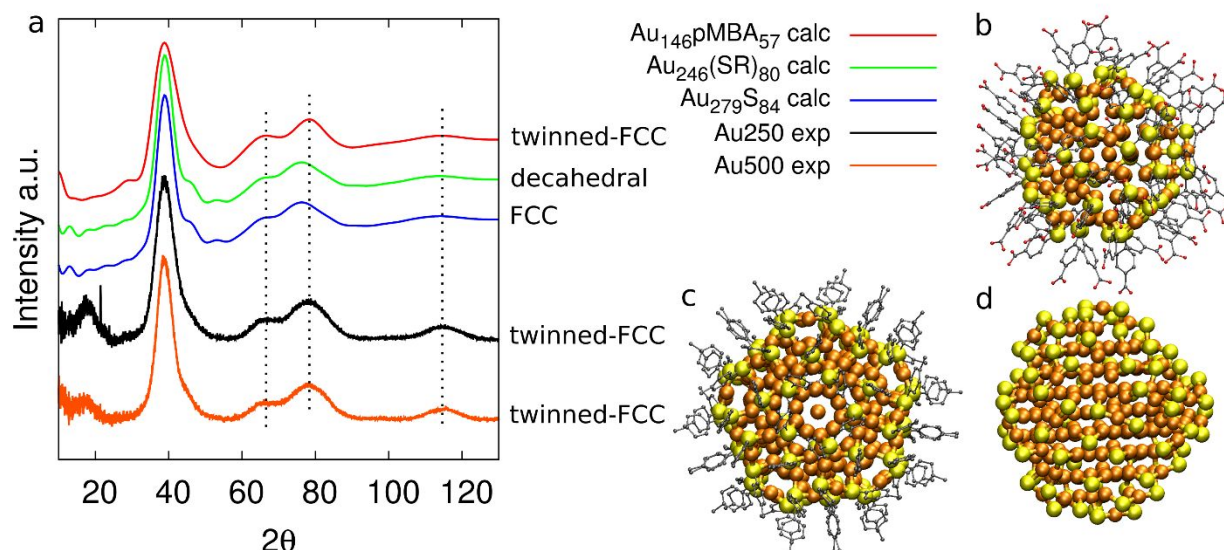


**Figure 6.** a) Diffraction patterns of the nanoclusters. Comparison of the experimental patterns of Au<sub>250</sub> (black line) and Au<sub>500</sub> (orange line) to the calculated patterns of Au<sub>146</sub>, Au<sub>246</sub>, and Au<sub>279</sub> clusters. The diffraction hump and very sharp peak at 20° 2θ in experimental patterns are caused by the sampler holder and the adhesive used for attaching the samples to the holder. Structural models of b) Au<sub>146</sub>(pMBA)<sub>57</sub> c) Au<sub>246</sub>(SR)<sub>80</sub> and d) Au<sub>279</sub>S<sub>84</sub>.

### Building model for twinned FCC metal core structures of Au<sub>250</sub> and Au<sub>500</sub>

Based on the obtained information from powder XRD analysis we start evaluating possible basis for metal core structure of Au<sub>250</sub> and Au<sub>500</sub> nanoclusters. Ranges of

possible candidates with the same twinned-FCC arrangement are shown in Figure 7.

The size range of the clusters was estimated based on PAGE. Furthermore, the estimated diameters of the clusters from HR-TEM,  $1.7\pm 0.1$  nm for Au<sub>250</sub> and  $2.2\pm 0.1$  nm for Au<sub>500</sub> are in agreement with modelled metal core of Au<sub>201</sub> and Au<sub>405</sub>, respectively. Therefore, we believe that they are possible candidates to start building structural model of the synthesized clusters.

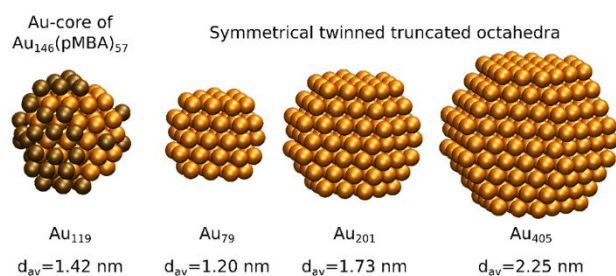


**Figure 7.** The range for possible basis for metal core structure in twinned FCC octahedral arrangement. Orange color represents gold atoms and brown color represents the additional layer of atoms on top of symmetrical Au<sub>79</sub> (left) representing together the Au-core of Au<sub>146</sub>(pMBA)<sub>57</sub>.

### HR-TEM image versus twinned-FCC core

1  
2  
3  
4 HR-TEM images represent further the symmetries of the AuMPCs. The simulated HR-  
5  
6  
7 TEM images of Au<sub>201</sub> metal core clearly support the imaging experiments of Au<sub>250</sub>  
8  
9  
10 (Figure 8). The observation of the lattice fringes in Figure 8 c) clearly shows the effects  
11  
12  
13 that can be only seen in both, FCC and twinned-FCC arrangements. The experimental  
14  
15  
16 figure 8 c) shows 7-9 rows of atomic layer giving excellent estimation of structural  
17  
18  
19 information at atomic resolution. The uncertainty in image interpretation is often due to  
20  
21  
22 poor contrast and number of interferences. Therefore, we simulated images of Au<sub>201</sub>  
23  
24  
25 metal core and compared them with our experimental findings. In the simulated image,  
26  
27  
28 there are 7 rows of the atomic layer (Fig. 8 c). The simulated images contain only the  
29  
30  
31 metal core atoms and the question arises how protected is the gold core under electron  
32  
33  
34 beam. In other words, for the analysis it is important to know whether the Au-S layer  
35  
36  
37 protecting the gold core is visible in the HR-TEM images. Simulated HR-TEM images  
38  
39  
40 and experimental equivalents Figure 8 a), b), d) show the effects that are reproducible  
41  
42  
43 only with the stacking fault defect for FCC-symmetry. Nevertheless, the symmetry found  
44  
45  
46 from powder XRD and HR-TEM are the same, which indicates that the core structure  
47  
48  
49 will remain the same under electron beam.  
50  
51  
52  
53  
54  
55  
56  
57  
58  
59  
60

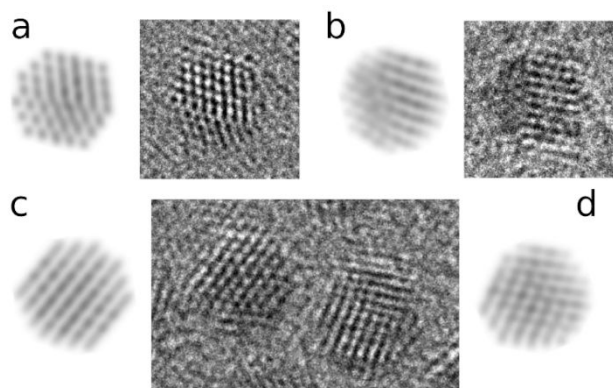


**Figure 8.** Comparison of HR-TEM images of Au<sub>250</sub> and simulated images of Au<sub>201</sub> metal core from different directions.

### 3.4. Predicting molecular composition

There is enough complementary experimental information for attempting determination of the molecular composition of the investigated clusters. Herein, we provide computationally aided predictions for the molecular compositions by reflecting the measured results of the synthesized clusters to the properties of selected, structurally known, thiolate protected clusters of a similar size. Selected known reference systems include clusters with close to spherical shape such as Au<sub>102</sub>(pMBA)<sub>44</sub>, Au<sub>146</sub>(pMBA)<sub>57</sub>, Au<sub>246</sub>(SC<sub>6</sub>H<sub>4</sub>CH<sub>3</sub>)<sub>80</sub> and Au<sub>271</sub>(TBBT)<sub>84</sub>, matching the

1  
2  
3 overall shape of the synthesized  $p$ MBA-protected particles. The clusters are selected  
4  
5  
6  
7 from the size range from 100 - 300 including the two known  $p$ MBA-clusters. Due to the  
8  
9  
10 absence of experimentally resolved structures of larger size water-soluble clusters, we  
11  
12  
13 included two of the largest thiolate protected clusters, despite of them being protected  
14  
15  
16  
17 with different type of aromatic ligands.  
18  
19

20  
21 By assuming  $p$ MBA-ligand for the selected known cluster compositions, trends of  
22  
23  
24 theoretical TG weight loss percentages can be predicted with the respect to the number  
25  
26  
27 of Au-atoms and the number of ligands as shown in Figure 9. Behavior shown in the  
28  
29  
30 figure is quite monotonous and by assuming that the behavior is valid also for the  
31  
32  
33 synthesized clusters, the composition  $Au_{210}(pMBA)_{72}$  can be predicted for the smaller  
34  
35  
36 cluster. Noteworthy is, that this composition would match perfectly with the magic  
37  
38  
39 electron shell closing of spherical clusters at 138 e, by assuming that gold provides 210  
40  
41  
42 Au(6s)-based free electrons to the system and the Au- $p$ MBA bonding withdraws 72  
43  
44  
45 electrons out from the system.<sup>46</sup>  
46  
47  
48  
49  
50  
51  
52  
53  
54  
55  
56  
57  
58  
59  
60

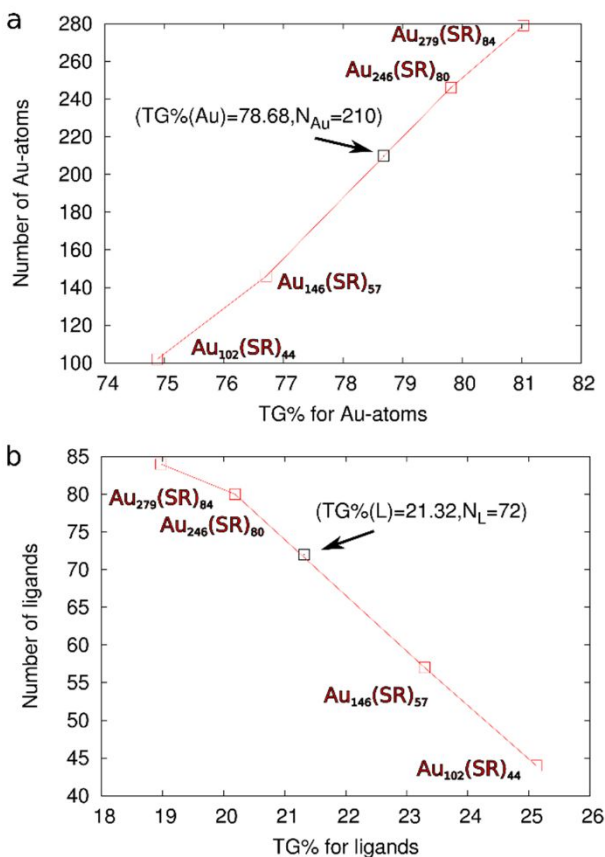


**Figure 9.** a) Number of Au-atoms in the thiolated clusters as a function of theoretically calculated thermogravimetric (TG) weight loss percentages of Au content. b) Number of ligands in the thiolated clusters as a function of theoretically calculated ligand TG percentages. Both are drawn using *p*MBA-ligand.

The second method for size estimation is based on the diameters of the clusters determined from the HR-TEM images the probable sizes of the metal core of the clusters can be estimated computationally. Figure 10 shows the number of metal atoms as a function of diameter as calculated for bare metal clusters of twinned-FCC symmetry. Model clusters were generated as described in Methods section. Using the

1  
2  
3  
4 experimentally measured diameters, the two synthesized clusters have approximately  
5  
6  
7  $187\pm 30$  and  $385\pm 50$  Au-atoms in their metal cores based on the correlation shown in  
8  
9  
10 Figure 10. The number of metal atoms in the Au-S interface varies from 23 to 40 in case  
11  
12  
13 of the selected four known reference clusters. Assuming further that 30-40 Au-atoms  
14  
15  
16 would participate on protecting units, the smaller synthesized particle would have  
17  
18  
19 approximately 220-230 Au-atoms in total depending on the actual Au-S interface  
20  
21  
22 conformation. Furthermore, we can estimate that at least 40 Au-atoms should be  
23  
24  
25 contributing to the Au-S interface of the larger synthesized cluster increasing the size to  
26  
27  
28  
29  
30  
31  $>425$  Au-atoms in total.  
32  
33  
34  
35  
36  
37  
38  
39  
40  
41  
42  
43  
44  
45  
46  
47  
48  
49  
50  
51  
52  
53  
54  
55  
56  
57  
58  
59  
60

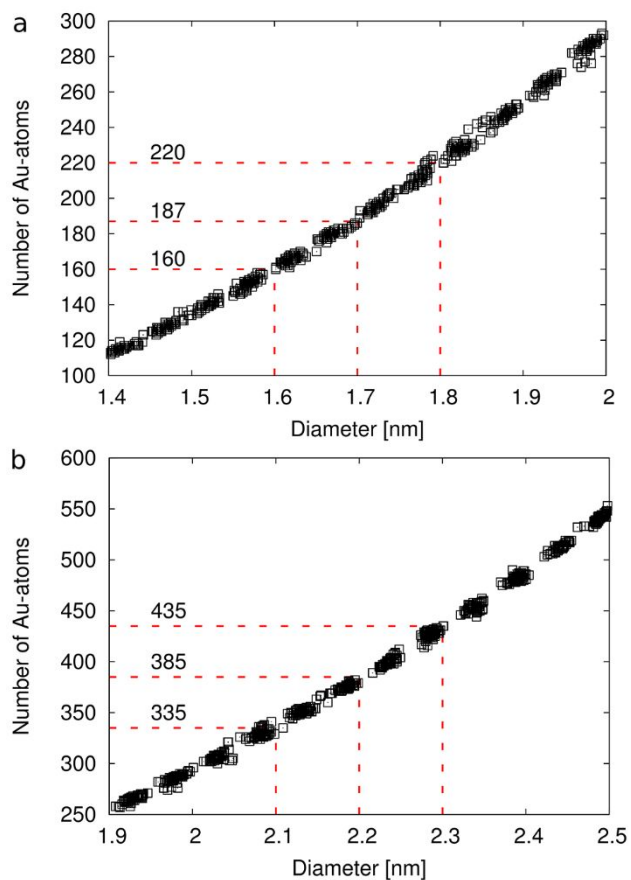
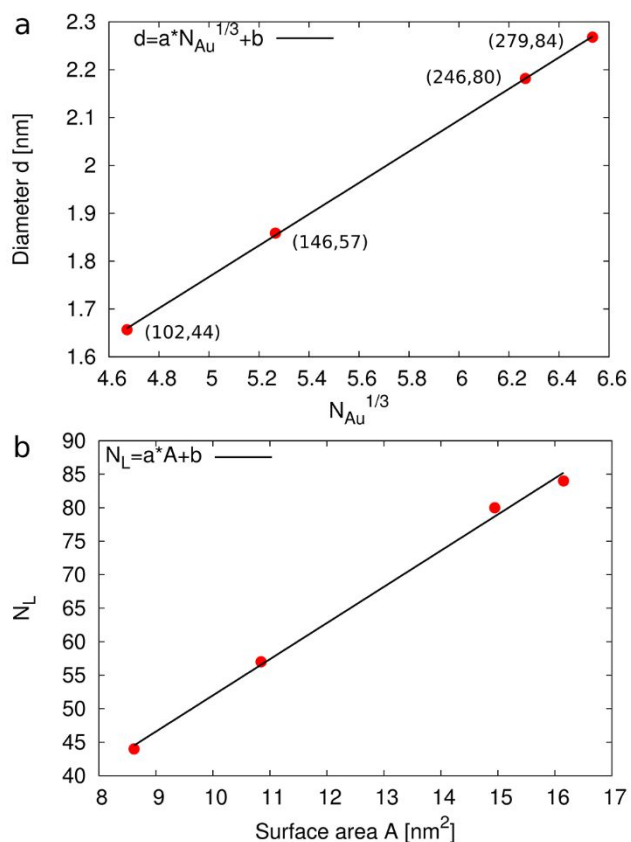


**Figure 10.** Number of Au-atoms of the spherical bare twinned-FCC Au-clusters in the size range relevant for the investigated  $\rho$ MBA-clusters in a) and b). The plausible sizes 187 and 385 of the metal core for the measured diameters are labeled in the figure. Based on the 0.1 nm error limits the minimum and maximum values are also given.

Third, we did linear fitting on the properties of the selected known clusters. We correlated the diameter of the cluster including metal core and Au-S interface to the



1  
2  
3 number of gold atoms in the cluster as shown in Figure 11 a). We also correlated the  
4  
5  
6  
7 number of ligands in the cluster to the spherical surface area as shown in Figure 11 b).  
8  
9  
10 The two linear correlations can be used to predict the molecular composition by relying  
11  
12  
13  
14 on experimentally measured diameters or on the estimated total number of gold atoms  
15  
16  
17 in the synthesized clusters.  
18  
19  
20  
21  
22  
23



51 **Figure 11.** a) Linear fitting done by correlating the number of Au-atoms in the cluster to  
52 the diameter of the cluster taking into account the metal core and Au-S interface atoms  
53  
54  
55  
56  
57  
58  
59  
60

1  
2  
3 and b) by correlating the corresponding spherical surface area to the number of ligands.  
4  
5

6  
7 Fitted parameters: a)  $a = 0.328 \text{ nm}$ ,  $b = 0.129 \text{ nm}$  and b)  $a = 5.40 \text{ nm}^{-2}$ ,  $b = -2.02$ .  
8  
9

10 Diameters of the clusters are determined including Au-core and Au-S interface as  
11  
12  
13  
14 described in Methods section.  
15  
16  
17  
18  
19

20 For the smaller Au<sub>250</sub> cluster the size range from 210-230 Au-atoms was already  
21  
22  
23 estimated to be realistic. Fixing the number of gold atoms to 210 gives as a prediction  
24  
25  
26 2.1 nm diameter for the cluster (including the metal core and the Au-S interface) and  
27  
28  
29 further 71 ligands for the protecting layer. Both are in agreement with the experimentally  
30  
31  
32 measured results. For example, the 1.7 nm diameter of the metal core should be  
33  
34  
35 increased at maximum twice the Au-S bond (0.235 nm) when adding the metal ligand  
36  
37  
38 interface. With the same procedure the upper size limit for the number of gold atoms at  
39  
40  
41  
42  
43  
44 230 gives a prediction of 2.1 nm diameter and 75 ligands, for which the closest  
45  
46  
47 composition matching the measured TG-percentages would be Au<sub>230</sub>(pMBA)<sub>80</sub>.  
48  
49  
50

51 For the larger Au<sub>500</sub> cluster prediction of the molecular composition can be also  
52  
53  
54 made although the reliability is not equally good due to the lack of reference structures.  
55  
56  
57  
58  
59  
60

1  
2  
3 For the larger cluster we take the measured diameter 2.2 nm of the core and add to it  
4  
5  
6  
7 approximately 0.4 nm from the metal-ligand interface. For the 2.6 nm spherical particle  
8  
9  
10 correlations predict that the total number of Au-atoms should be 429 and the number of  
11  
12  
13 ligands 113. Molecular composition would be  $\text{Au}_{429}(\text{SR})_{113}$  which has a very good match  
14  
15  
16 with the measured TG weight loss percentages. All the nearby compositions within 0.1  
17  
18  
19 TG-percentage units from the measured results are included in compositions  $\text{Au}_{426-}$   
20  
21  
22  $442(\rho\text{MBA})_{112-115}$ . The prediction of 426-442 gold atoms in total is reasonable as  
23  
24  
25 compared to the estimated core size of 385 Au-atoms, which would mean that 40-60  
26  
27  
28 Au-atoms were included in the protecting units. The number of single bridged ligands, not  
29  
30  
31 resembling a conformation of any protecting unit, increases in the Au-S interface as the cluster  
32  
33  
34 size increases. This can be realized by analyzing the structures of the known reference clusters  
35  
36  
37  $\text{Au}_{102}(\text{SR})_{44}$ ,  $\text{Au}_{146}(\text{SR})_{57}$ ,  $\text{Au}_{246}(\text{SR})_{80}$  and  $\text{Au}_{279}(\text{SR})_{84}$ . Their Au-S interfaces include  
38  
39  
40 respectively 0% (0/44), 12.3% (7/57), 12.5% (10/80) and 21.4% (18/84) of bridged ligands. At  
41  
42  
43 the same time the relative number of Au-atoms in the Au-S interface decreases as the cluster size  
44  
45  
46 increases, at least within the represented size range.

47  
48  
49 As a summary, the best computationally aided predictions for the molecular  
50  
51  
52 compositions are  $\text{Au}_{210-230}(\rho\text{MBA})_{70-80}$  for the smaller cluster and  $\text{Au}_{426-442}(\rho\text{MBA})_{112-115}$   
53  
54  
55 for the larger cluster.  
56  
57  
58  
59  
60

#### 4. CONCLUSION

In this work, we synthesized, in milligram scale, stable sizes of water-soluble  $\rho$ MBA-protected gold nanoclusters by controlling the pH in different MeOH/H<sub>2</sub>O conditions. The products were carefully analyzed by various analytical techniques and characterized for approximate mass and structural composition. So far, water-soluble clusters have been observed in decahedral (Au<sub>102</sub>( $\rho$ MBA)<sub>44</sub>),<sup>45</sup> FCC-like (Au<sub>68</sub>( $m$ MBA)<sub>32</sub> and Au<sub>144</sub>( $m$ MBA)<sub>n</sub>)<sup>38</sup> and twinned-FCC (Au<sub>146</sub>( $\rho$ MBA)<sub>57</sub>) symmetries<sup>41</sup>. The results in this paper indicate that twinned-FCC symmetry is favored in larger  $\rho$ MBA-protected clusters as shown in the case of Au<sub>250</sub> and Au<sub>500</sub>. Combining all the experimental information and computational analysis we came to the final prediction of the molecular composition of the synthesized clusters, namely Au<sub>210-230</sub>( $\rho$ MBA)<sub>70-80</sub> and Au<sub>426-442</sub>( $\rho$ MBA)<sub>112-115</sub>. The structural knowledge of these clusters is crucial when applying these to biological studies. There is still a lack of well-defined, water-soluble particles, which could serve as universal labeling tools for bioimaging. Attaching gold

1  
2  
3 nanoclusters to the biological systems will allow the investigation of viruses, including  
4  
5  
6  
7 their entry mechanism into cells. The development of cluster-based sensors by  
8  
9  
10 chemically modifying the ligand layer of the water-soluble gold nanoclusters is one of  
11  
12  
13 the possibilities to achieve controllable application in biosciences and to study for  
14  
15  
16  
17 example the nature of viral genome release in cells (during infection). In addition, in the  
18  
19  
20 field of spectroscopy in physical chemistry, the plasmonic nanoclusters are important  
21  
22  
23 model systems to study emergence of bulk properties in metal and using them as a  
24  
25  
26  
27 building blocks could give deepen understanding of energy transfer processes, which  
28  
29  
30 are of interest in molecular electronics.  
31  
32  
33

34  
35 This work introduces some overall trends in synthetic methods and structural  
36  
37  
38 compositions for two larger water-soluble AuMPCs. These play a crucial role in  
39  
40  
41 understanding the relation of their diverse properties and increase the usability of gold  
42  
43  
44  
45 nanoclusters.  
46  
47  
48  
49  
50  
51

## 52 ASSOCIATED CONTENT

53  
54  
55  
56  
57  
58  
59  
60

1  
2  
3 **Supporting Information.** Supporting Information is available free of charge on the ACS  
4  
5  
6

7 Publications website at DOI  
8  
9

10  
11 Detailed experimental procedures and methods for prediction of molecular  
12  
13 composition; PAGE gel showing fractional precipitation procedure; TEM images taken  
14  
15 from Au250 and Au500 nanoclusters; full spectrum of  $^1\text{H}$  NMR of Au250 and Au500  
16  
17 nanoclusters; Image of the residual after TG run. This material is available free of  
18  
19 charge via the Internet at [http:](http://)  
20  
21  
22  
23  
24  
25  
26  
27  
28  
29  
30  
31

## 32 **AUTHOR INFORMATION**

33  
34  
35

### 36 **Corresponding Author**

37  
38  
39

40 \*E-mail: [tanja.m.lahtinen@jyu.fi](mailto:tanja.m.lahtinen@jyu.fi). Phone: +358 40805 3697 (T.L.).  
41  
42  
43  
44

### 45 **ORCID**

46  
47

48 Tanja Lahtinen: 0000-0002-1747-6959; Hannu Häkkinen: 0000-0002-8558-5436  
49  
50

### 51 **Notes**

52  
53  
54  
55  
56  
57  
58  
59  
60

1  
2  
3 The authors declare no competing financial interest.  
4  
5  
6  
7  
8

9  
10 **ACKNOWLEDGMENT**  
11

12  
13 We acknowledge Aalto University for the access to HR-TEM facilities and technical  
14  
15  
16 support.  
17  
18  
19

20  
21 **Funding Sources**  
22

23  
24  
25 This work was financially supported by the Academy of Finland via projects 269402,  
26  
27  
28 273499, 303753 (L.L.), 252411, 297049, 292352 (H.H.), 294217 (H.H), and Emil  
29  
30  
31  
32 Aaltonen Foundation grant to M.J.  
33  
34  
35  
36  
37

38 **REFERENCES**  
39  
40

41  
42 (1) Salorinne, K.; Lahtinen, T.; Malola S.; Koivisto, J.; Häkkinen, H. Solvation  
43  
44  
45 Chemistry of Water-Soluble Thiol Protected Gold Nanocluster Au<sub>102</sub> from DOSY NMR  
46  
47  
48 Spectroscopy and DFT Calculations. *Nanoscale* **2014**, *6*, 7823.  
49  
50  
51  
52  
53  
54  
55  
56  
57  
58  
59  
60

1  
2  
3  
4 (2) Plascencia-Villa, G.; Demeler, B.; Whetten, R.L.; Griffith, W.P.; Alvarez, M.; Black,  
5  
6  
7 D.M.; José-Yacamán, M. Analytical Characterization of Size-Dependent Properties of  
8  
9  
10 Larger Aqueous Gold Nanoclusters. *J. Phys. Chem. C* **2016**, *120*, 8950–8958.

11  
12  
13  
14  
15 (3) Jin, R. Atomically precise metal nanoclusters: stable sizes and optical properties.  
16  
17  
18 *Nanoscale* **2015**, *7*, 1549.

19  
20  
21  
22 (4) Marjomäki, V.; Lahtinen, T.; Martikainen, M.; Koivisto, J.; Malola, S.; Salorinne, K.;  
23  
24  
25  
26 Pettersson, M.; Häkkinen, H. *Proc. Natl. Acad. Sci. U. S. A.*, **2014**, *111*, 1277–1281.

27  
28  
29  
30 (5) Homberger, M.; Simon, U. On the Application Potential of Gold Nanoparticles in  
31  
32  
33  
34 Nanoelectronics and Biomedicine. *Philos. Trans. R. Soc., A* **2010**, *368*, 1405–1453.

35  
36  
37  
38 (6) Nie, S.; Emory, S. R. Probing Single Molecules and Single Nanoparticles by  
39  
40  
41  
42 Surface- Enhanced Raman Scattering. *Science* **1997**, *275*, 1102–1106.

43  
44  
45  
46 (7) Brongersma, M. L.; Halas, N. J.; Nordlander, P. Plasmon-Induced Hot Carrier  
47  
48  
49  
50 Science and Technology. *Nat. Nanotechnol.* **2015**, *10*, 25– 34.



- 1  
2  
3 (8) Tapio, K.; Leppiniemi, J.; Shen, B.; Hytönen, V. P.; Fritzsche, W.; Toppari, J. J.  
4  
5  
6  
7 Toward Single Electron Nanoelectronics Using Self- Assembled DNA Structure. *Nano*  
8  
9  
10 *Lett.* **2016**, *16*, 6780–6786.  
11  
12  
13  
14 (9) Martikainen, M.; Salorinne, K.; Lahtinen, T.; Malola, S.; Permi, P.; Häkkinen, H.;  
15  
16  
17  
18 Marjomäki, V.; Hydrophobic pocket targeting probes for enteroviruses. *Nanoscale* **2015**,  
19  
20  
21 *7*, 17457.  
22  
23  
24  
25 (10) Stark, M.C.; Baikoghli, M.A.; Lahtinen, T.; Malola, S.; Xing, L.; Nguyen, M.;  
26  
27  
28  
29 Nguyen, M.; Sikaroudi, A.; Marjomäki, V.; Häkkinen, H.; et al. Structural  
30  
31  
32  
33 Characterization of Site-Modified Nanocapsid with Monodispersed Gold Clusters.  
34  
35  
36 *Scientific Reports* **2017**, *7*, 1-11.  
37  
38  
39  
40 (11) Calard, F.; Wani, I.H.; Hayat, A.; Jarrosson, T.; Lère-Porte, J.-P.; Jafri, S.H.M.;  
41  
42  
43  
44 Serein-Spirau, F.; Leifer, K.; Orthaber, A. Designing Sterically Demanding Thiolate  
45  
46  
47  
48 Coated AuNPs for Electrical Characterization of BPDT in a NP–Molecule–  
49  
50  
51 Nanoelectrode Platform. *Mol. Syst. Des. Eng.* **2017**, *2*, 133.  
52  
53  
54  
55  
56  
57  
58  
59  
60

1  
2  
3  
4 (12) Häkkinen, H. The Gold-Sulfur Interface at the Nanoscale. *Nat. Chem.*, **2012**, *4*,  
5  
6  
7 443–455.  
8  
9

10  
11 (13) Jin, R.; Zeng, C.; Zhou M.; Chen, Y. Atomically Precise Colloidal Metal Nanoclusters  
12  
13  
14 and Nanoparticles: Fundamentals and Opportunities. *Chem. Rev.* **2016**, *116*, 10346–10413.  
15  
16  
17

18  
19 (14) Chakraborty, I.; Pradeep, T. Atomically Precise Clusters of Noble Metals:  
20  
21  
22 Emerging Link between Atoms and Nanoparticles. *Chem. Rev.* **2017**, *117*, 8208–8271.  
23  
24  
25

26  
27 (15) Sakthivel, N.A.; Theivendran, S; Ganeshraj, V.; Oliver, A.G.; Dass, A. Crystal  
28  
29  
30 Structure of Faradaurate-279: Au<sub>279</sub>(SPh-tBu)<sub>84</sub> Plasmonic Nanocrystal Molecules. *J.*  
31  
32  
33  
34 *Am. Chem. Soc.* **2017**, *139*, 15450-15459.  
35  
36  
37

38  
39 (16) Kumara, C.; Zuo, X.; Ilavsky, J.; Chapman, K.-W.; Cullen, D.-A.; Dass, A. Super-  
40  
41  
42 Stable Highly Monodisperse Plasmonic Faradaurate-500 Nanocrystals with 500 Gold  
43  
44  
45 Atoms: Au<sub>~500</sub>(SR)<sub>~120</sub>. *J. Am. Chem. Soc.* **2014**, *136*, 7410-7417.  
46  
47  
48  
49  
50  
51  
52  
53  
54  
55  
56  
57  
58  
59  
60

1  
2  
3  
4 (17) Jin, R.; Qian, H.; Wu, Z.; Zhu, Y.; Zhu, M.; Mohanty, A.; Garg, N. Size Focusing:  
5  
6  
7 A Methodology for Synthesizing Atomically Precise Gold Nanoclusters. *J. Phys. Chem.*  
8  
9  
10 *Lett.*, **2010**, *1*, 2903–2910.

11  
12  
13  
14 (18) Qian, H.; Zhu, Y., Jin, R. Size-Focusing Synthesis, Optical and Electrochemical  
15  
16  
17  
18 Properties of Monodisperse  $\text{Au}_{38}(\text{SC}_2\text{H}_4\text{Ph})_{24}$  Nanoclusters. *ACS Nano* **2009**, *3*,  
19  
20  
21 3795–3803.

22  
23  
24  
25 (19) Qian, H.; Zhu, Y., Jin, R. Atomically Precise Gold Nanocrystal Molecules with  
26  
27  
28  
29 Surface Plasmon Resonance. *Proc.Natl.Acad.Sci.U.S.A.* **2012**, *109*, 696–700.

30  
31  
32  
33 (20) Qian, H.; Jin, R. Ambient Synthesis of  $\text{Au}_{144}(\text{SR})_{60}$  Nanoclusters in Methanol.  
34  
35  
36  
37 *Chem. Mater.* **2011**, *23*, 2209–2217.

38  
39  
40  
41 (21) Schaff, T.; Whetten, R. Controlled Etching of Au:SR Cluster Compounds. *J. Phys.*  
42  
43  
44  
45 *Chem. B* **1999**, *103*, 9394–9396.

1  
2  
3  
4 (22) Dharmaratne, A. C.; Krick, T.; Dass, A. Nanocluster Size Evolution Studied by  
5  
6  
7 Mass Spectrometry in Room Temperature  $\text{Au}_{25}(\text{SR})_{18}$  Synthesis. *J. Am. Chem. Soc.*  
8  
9  
10 **2009**, *131*, 13604–13605.

11  
12  
13  
14 (23) Negishi, Y.; Nakazaki, T.; Malola, S.; Takano, S.; Niihori, Y.; Kurashige, W.;  
15  
16  
17 Yamazoe, S.; Tsukuda T.; Häkkinen, H. A Critical Size for Emergence of Nonbulk  
18  
19  
20  
21 Electronic and Geometric Structures in Dodecanethiolate-Protected Au Clusters. *J. Am.*  
22  
23  
24  
25 *Chem. Soc.* **2015**, *137*, 1206–1212.

26  
27  
28  
29 (24) Yi, C.; Zheng, H.; Tvedte, L.M.; Ackerson, C.J.; Knappenberger, K.L.J.  
30  
31  
32  
33 Nanometals: Identifying the Onset of Metallic Relaxation Dynamics in Monolayer-  
34  
35  
36  
37 Protected Gold Clusters Using Femtosecond Spectroscopy. *J. Phys. Chem. C* **2015**,  
38  
39  
40 *119*, 6307– 6313.

41  
42  
43  
44 (25) Lahtinen, T.; Hulkko, E.; Sokołowska, K.; Tero, T.-R.; Saarnio, V.; Lindgren, J.;  
45  
46  
47  
48 Pettersson, M.; Häkkinen, H.; Lehtovaara, L. Covalently Linked Multimers of Gold  
49  
50  
51  
52 Nanoclusters  $\text{Au}_{102}(\rho\text{MBA})_{44}$  and  $\text{Au}_{\sim 250}(\rho\text{MBA})_n$ . *Nanoscale* **2016**, *8*, 18665–18674.  
53  
54  
55  
56  
57  
58  
59  
60

1  
2  
3 (26) Yampolsky, S.; Fishman, D.A.; Dey, S.; Hulkko, E.; Banik, M.; Potma, E.O.;  
4  
5  
6  
7 Apkarian, V.A. Seeing a Single Molecule Vibrate Through Time-Resolved Coherent  
8  
9  
10 Anti-Stokes Raman Scattering. *Nature Phot.* **2014**, *8*, 650.

11  
12  
13  
14  
15 (27) Sels, A.; Salassa, G.; Cousin, F.; Lee, L.-T.; Bürgi, T. Covalently Bonded Multimers of  
16  
17  
18 Au<sub>25</sub>(SBut)<sub>18</sub> as a Conjugated System. *Nanoscale* **2018**, *10*, 12754.

19  
20  
21  
22 (28) Schaaff, T.; Knight, G.; Shafigullin, M.; Borkman, R.; Whetten, R. Isolation and  
23  
24  
25  
26 Selected Properties of a 10.4 kDa Gold:Glutathione Cluster Compound. *J. Phys. Chem.*  
27  
28  
29 *B* **1998**, *102*, 10643–10646.

30  
31  
32  
33 (29) Schaaff, T.; Whetten, R. Controlled Etching of Au:SR Cluster Compounds. *J.*  
34  
35  
36  
37 *Phys. Chem. B* **1999**, *103*, 9394–9396.

38  
39  
40  
41 (30) Dass, A. Faradaurate Nanomolecules: A Superstable Plasmonic 76.3 kDa  
42  
43  
44  
45 Cluster. *J. Am. Chem. Soc.*, **2011**, *133*, 19259–19261.

46  
47  
48  
49 (31) Alvarez, M.M.; Chen, J.; Plascencia-Villa, G.; Black, D.M.; Griffith, W.P.; Garzon,  
50  
51  
52  
53 I.L.; Jose-Yacamán M.; Demeler, B.; Whetten, R.L. Hidden Components in Aqueous  
54  
55  
56  
57  
58  
59  
60

1  
2  
3  
4 “Gold-144” Fractionated by PAGE: High-Resolution Orbitrap ESI-MS Identifies the Gold-  
5  
6  
7 102 and Higher All-Aromatic Au-pMBA Cluster Compounds. *J. Phys. Chem. B* **2016**,  
8  
9  
10 *120*, 6430–6438.

11  
12  
13  
14  
15 (32) Plascencia-Villa, G.; Demeler, B; Whetten, R.L.; Griffith, W.P.; Alvarez, M.; Black,  
16  
17  
18 D.M.; Jose-Yacaman, M. Analytical Characterization of Size-Dependent Properties of  
19  
20  
21 Larger Aqueous Gold Nanoclusters. *J. Phys. Chem. C* **2016**, *120*, 8950–8958.

22  
23  
24  
25  
26 (33) Tvedte, L.M.; Ackerson, C.J. Size-Focusing Synthesis of Gold Nanoclusters with *p*-  
27  
28  
29 Mercaptobenzoic Acid. *J. Phys. Chem. A* **2014**, *118*, 8124–8128.

30  
31  
32  
33  
34 (34) Levi-Kalisman, Y.; Jadzinsky, P. D.; Kalisman, N.; Tsunoyama, H.; Tsukuda, T.;  
35  
36  
37 Bushnell, D. A.; Kornberg, R. D. Synthesis and Characterization of Au<sub>102</sub>(pMBA)<sub>44</sub>  
38  
39  
40 Nanoparticles. *J. Am. Chem. Soc.* **2011**, *133*, 2976–2982.

41  
42  
43  
44  
45 (35) Ackerson, C. J.; Jadzinsky, P. D.; Sexton, J. Z.; Bushnell, D. A.; Kornberg, R. D.  
46  
47  
48 Synthesis and Bioconjugation of 2 and 3 nm-Diameter Gold Nanoparticles.  
49  
50  
51 *Bioconjugate Chem.* **2010**, *21*, 214–218.

1  
2  
3  
4 (36) Wong, O.A.; Compel, W.S.; Ackerson, C.J. Combinatorial Discovery of Cosolvent  
5  
6  
7 Systems for Production of Narrow Dispersion Thiolate-Protected Gold Nanoparticles.  
8  
9  
10 *ACS Comb. Sci.* **2015**, *17*, 11–18.

11  
12  
13  
14 (37) Azubel, M.; Kornberg, R.D. Synthesis of Water-Soluble, Thiolate-Protected Gold  
15  
16  
17 Nanoparticles Uniform in Size. *Nano Lett.* **2016**, *16*, 3348–3351.

18  
19  
20  
21 (38) Azubel, M.; Koivisto, J.; Malola, S.; Bushnell, D.; Hura, G.L.; Koh, A.-L.;  
22  
23  
24  
25  
26 Tsunoyama, H.; Tsukuda, T.; Pettersson, M.; Häkkinen, H.; et al. Electron Microscopy  
27  
28  
29 of Gold Nanoparticles at Atomic Resolution. *Science* **2014**, *6199*, 909-912.

30  
31  
32  
33 (39) Tero, T.-R.; Malola S., Koncz, B.; Pohjolainen, E.; Lautala, S.; Mustalahti, S.; Permi,  
34  
35  
36 P.; Groenhof, G.; Pettersson, M.; Häkkinen, H. Dynamic Stabilization of the Ligand–Metal  
37  
38 Interface in Atomically Precise Gold Nanoclusters Au<sub>68</sub> and Au<sub>144</sub> Protected by *meta*-  
39  
40 Mercaptobenzoic Acid. *ACS Nano* **2017**, *11*, 11872–11879.

41  
42  
43 (40) Azubel, M.; Koh, A.-L.; Koyasu, K.; Tsukuda, T.; Kornberg, R.-D. Structure  
44  
45  
46  
47 Determination of a Water-Soluble 144-Gold Atom Particle at Atomic Resolution by  
48  
49  
50  
51 Aberration-Corrected Electron Microscopy. *ACS Nano* **2017**, *11*, 11866–11871.

1  
2  
3 (41) Vergara, S.; Lukes, D.A.; Martynowycz, M.W.; Santiago, U.; Plascencia-Villa,  
4 G.; Weiss, S.C.; Cruz, M.J.; Black, D.M.; Alvarez, M.M.; López-Lozano, X.; et al. MicroED  
5 Structure of Au<sub>146</sub>(pMBA)<sub>57</sub> at Subatomic Resolution Reveals a Twinned FCC Cluster *J. Phys.*  
6 *Chem. Lett.*, **2017**, *8*, 5523–5530.  
7  
8  
9

10  
11  
12  
13 (42) Sokołowska, K.; Hulkko, E.; Lehtovaara, L.; Lahtinen, T. Dithiol-Induced  
14 Oligomerization of Thiol-Protected Gold Nanoclusters *J. Phys. Chem. C* **2018**, *122*,  
15 12524–12533.  
16  
17  
18  
19  
20  
21  
22

23  
24 (43) International Centre for Diffraction Data, ICDD-PDF4+. <http://www.icdd.com/>  
25  
26  
27  
28 (accessed December 10, 2018).  
29  
30  
31

32 (44) Lopez-Acevedo, O.; Akola, J.; Whetten, R.L.; Grönbeck, H.; Häkkinen, H.  
33 Structure and Bonding in the Ubiquitous Icosahedral Metallic Gold Cluster Au<sub>144</sub>(SR)<sub>60</sub>.  
34  
35  
36  
37  
38  
39  
40 *J. Phys. Chem. C* **2009**, *113*, 5035.  
41  
42

43 (45) Jadzinsky, P.D.; Calero, G; Ackerson, C.J.; Bushnell, D.A.; Kornberg, R.D.  
44 Structure of a Thiol Monolayer-Protected Gold Nanoparticle at 1.1 Å Resolution.  
45  
46  
47  
48  
49  
50  
51 *Science* **2007**, *318*, 430-433.  
52  
53  
54  
55  
56  
57  
58  
59  
60



(46) Walter, M.; Akola, J.; Lopez-Acevedo, O.; Jadzinsky, P.-D.; Calero, G.; Ackerson, C.-J.; Whetten, R.-L.; Grönbeck, H.; Häkkinen, H.; A Unified View of Ligand-Protected Gold Clusters as Superatom Complexes. *Proc.Natl.Acad.Sci.U.S.A.* **2008**, *105*, 9157-9162.

### TOC Graphic

